Available online at www.sciencedirect.com

ScienceDirect

Procedia Computer Science 100 (2016) 1181 – 1190

Procedia Computer Science

Conference on ENTERprise Information Systems / International Conference on Project MANagement / Conference on Health and Social Care Information Systems and Technologies, CENTERIS / ProjMAN / HCist 2016, October 5-7, 2016

Multi-Temporal InSAR processing comparison in presence of high topography

Antonio M. Ruiz-Armenteros[a,b,c,*], Matus Bakon[d], Milan Lazecky[e], J. Manuel Delgado[c,f] Joaquim J. Sousa[g], Daniele Perissin[h] and Miguel Caro-Cuenca[i]

[a]*Dpto. Ingeniería Cartográfica, Geodésica y Fotogrametría, Univ. Jaén, EPSJ, Campus Las Lagunillas s/n, Edif. A3, 23071 Jaén, Spain*
[b]*Centro de Estudios Avanzados en Ciencias de la Tierra CEACTierra, Universidad de Jaén, Spain*
[c]*Grupo de investigación Microgeodesia Jaén, Universidad de Jaén, Spain*
[d]*Department of Theoretical Geodesy, Slovak University of Technology, Radlinskeho 11, 810 05 Bratislava, Slovakia*
[e]*IT4Innovations, VSB-TU Ostrava, Czech Republic*
[f]*Progressive Systems Srl, Rome, Italy*
[g]*UTAD, Vila Real and INESC-TEC (formerly INESC Porto), Portugal*
[h]*School of Civil Engineering, Purdue University, 550 Stadium Mall Drive, West Lafayette, IN47907, Office: HAMP 4106, USA*
[i]*TNO, The Hague, The Netherlands*

Abstract

In this paper we compare the results obtained by three different InSAR tool packages, StaMPS, SARPROZ and P-SBAS (CNR-IREA) on G-POD for the processing of a mountainous area with up to 2,000 m high differences. For that we use two dataset ERS-1/2 and Envisat ASAR. The area (Sierra Tejeda, southern Spain) is located close to the coast line in the Internal Zone of the Betic Cordillera. The recent NW-SE convergence of the Eurasian-African plate boundary makes this area to belong to a large fold which continues active up to present. The uplift of the mountain ranges is mainly related to the development of folds in this regional compressive setting. This paper investigates and compares the velocity pattern obtained by the three different algorithms to help to constraint the geological hazard in this part of the Betic Cordillera.

Peer-review under responsibility of the organizing committee of CENTERIS 2016

Keywords: InSAR, Multi-Temporal InSAR, deformation monitoring, Betic Cordillera, Sierra Tejeda

* Corresponding author. Tel.: +34 953 212 851; fax: +34 953 212 854
E-mail address: amruiz@ujaen.es

Peer-review under responsibility of the organizing committee of CENTERIS 2016
doi:10.1016/j.procs.2016.09.278

1. Introduction

Measurements of crustal deformation are contributing greatly to our understanding of Earth dynamics, being it related with tectonic, seismic, volcanic activity or to landslides. Surface deformation measurements can be used to constrain the subsurface geometry of active faults and the spatial distribution of coseismic slip. Many measurement techniques have been developed over time to study the Earth's surface deformation. Some of these techniques, besides having different levels of accuracy, are very time consuming (e.g. classical surveys). One of the most recent and effective developed technique is the spaceborne Synthetic Aperture Radar Interferometry (InSAR), based on microwave pulses emitted by a spaceborne SAR instrument on board of a satellite.

In the late 1990s it was noticed that some radar targets maintain stable backscattering characteristics for a period of months or years (or even decades)[1,2], and the phase information from these stable targets (hereafter called Persistent Scatterers or PS) can be used, even over a long time period. The Multi-temporal InSAR (MT-InSAR) techniques represented an important advance with respect to the standard ones, both in terms of deformation modelling capabilities and quality of the deformation estimations. MT-InSAR techniques emerged and immediately gained popularity as a tool for deformation measurements due to its ability to overcome limitations of the conventional DInSAR: temporal and geometric decorrelation, and atmospheric inhomogeneities. Presently there are several MT-InSAR methods developed by different research groups that exploit data acquired by spaceborne SAR sensors with surface monitoring purposes. However, some of these methodologies, depending on the motivations that led to its development, present conceptual differences resulting in different level of performance. See[3], for instance, for a general review.

The deformation occurring in the Betic Cordillera (southern Spain) corresponds to the relative movement between Iberia and Africa plates. From the later Miocene to the present, their convergence (4 mm/year in a NW-SE direction[4]) mainly lead to a dynamic situation in which a NNW-SSE to NW-SE compression is combined with an ENE-WSW extension. As a consequence, some mountain ranges and, in particular, Sierra Tejeda (Fig. 1) located in the Internal zone of the Betic Cordillera was gently folded in an approximate E-W direction (as occurred in other areas in the Betics, for instance the great antiform of Sierra Nevada). The antiform of Sierra Tejeda is superposed to a very complicated Alpine structure, where very tight folds are abundant. Faults and folds contributed to the present elevation of Sierra Tejeda, giving a strong relief in comparison to the surrounding area (Fig. 2) with peaks around 2.000 m above mean sea level. [5]investigated the deformation pattern of this area of the Betic Cordillera in the period 1992-2008 by using satellite radar interferometry with ERS-1/2 and Envisat ASAR datasets. The most significant surprising result was that the main elevated areas (Sierra Gorda and Sierra Tejeda) undergone present-day subsidence for all the period in respect to the low relief areas (Granada basin at the north and southwestern Sierra Tejeda).

With the aim of monitoring ground deformation under unfavorable conditions caused by rough topography and millimetric deformation rates like the case of the main faults in the Betic Cordillera, in this paper we compare the processing results of this area with the cited dataset (ERS-1/2 and Envisat ASAR - 1992-2008) using three different InSAR tool packages: Stanford Method for Persistent Scatterers Multi-Temporal InSAR (StaMPS-MTI), SARPROZ, and the P-SBAS service by CNR-IREA[6] and ESA-RSS[7] within the ESA's G-POD (Grid Processing on Demand) platform.

2. Satellite datasets

The study area is covered by two different satellite tracks. Ground movements present in section 4 have been measured performing MT-InSAR on 36 ERS-1/2 C-band and 27 Envisat ASAR C-band SLC scenes (both ~5,7 cm wavelength). The ERS-1/2 data correspond to descending orbits (track 51) acquired between 05/05/199 and 28/12/2000 with an incident angle of 23º and a 5x25 m nominal spatial resolution. The Envisat ASAR images were acquired from 21/03/2003 to 01/08/2008, along descending orbits (track 459),with an incidence angle of 23º at the middle swath IS2, and a 5x25 m nominal pixel dimension. Fig. 1 shows the distribution of these tracks over the study area. Due to ERS-2 on-board gyroscope failure on January 2001, only images until the end of 2000 were selected to avoid high Doppler centroid differences of more than the critical value of 700 Hz. Master images were selected on 4th December 1998 for the ERS-1/2 dataset and on 5th November 2004 in the case of Envisat.

3. Multi-Temporal InSAR

InSAR is limited by temporal and geometrical decorrelation as mentioned before. MT-InSAR methods are helpful to overcome these limitations. The idea behind these methods is to discern coherent radar signal from incoherent contributions in order to obtain only those observations which are physically meaningful. In other words, a PS (Permanent or Persistent Scatterer) is an isolated point with interpretable phase characteristics in time. Methods for identifying and isolating these PS in interferograms have been developed using a functional model to map deformation variation with time. The methods have been very successful in identifying PS pixels in both urban and non-urban areas undergoing primarily steady-state or periodic deformation.

Currently, there are two broad categories of MT-InSAR techniques, persistent scatterer (PSI) methods (e.g.[8,9,10]) and small baseline (SB) methods (e.g.[11,12]). In the following subsections we briefly describe some characteristics of the used InSAR tool packages.

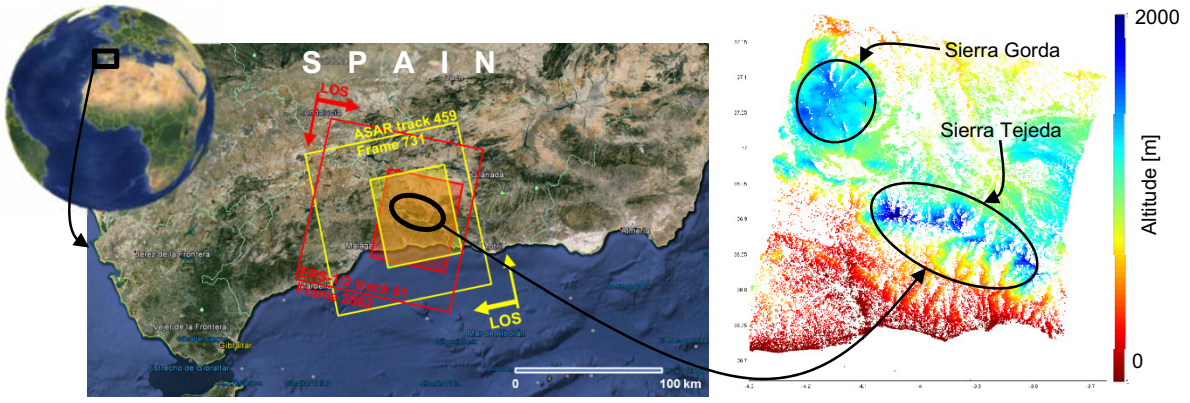

Fig. 1. Location of the study area (Sierra Tejeda in Betic Cordidllera, southern Spain). The AOI is depicted by a black ellipse in the middle figure where both the ascending and descending frames and cropped areas are shown by yellow and red rectangles respectively. On the right, a Digital Elevation Model (DEM) of the study area. Altitudes range from 0 to 2.000 m.

3.1. StaMPS

StaMPS is a software package developed in MATLAB® that implements a PSI method developed to work even in terrains devoid of man-made structures and/or undergoing non-steady deformation[13,14]. StaMPS-MTI (MT-InSAR) is an extended version of StaMPS that also includes an SB method and a combined MT-InSAR method, allowing the identification of scatterers that dominate the scattering from the resolution cell (PS) and slowly decorrelation-filtered phase (SDFP) pixels, that is, pixels whose phase when filtered decorrelates little over short time intervals[15].

The processing chain begins by reading the SAR scenes and precise orbits. Then, the master scene is selected in order to start the InSAR processing. Parameters such as the effective baseline, the acquisition date, the Doppler centroid frequency and the season of the acquisition, form the selection criteria. During the differential interferometric processing steps the observation geometry of the radar acquisition is simulated. A Digital Elevation Model (DEM) and precise orbits are used as input. That means that the interferometric phase can be modelled. The differential interferometric phase is used in all further computations.

StaMPS uses both amplitude and phase analysis to determine the PS probability for individual pixels. First an initial selection based only on amplitude analysis is performed, and then the PS probability is refined using phase analysis in an iterative process. Once selected, the signal due to deformation in the PS pixels is isolated. In contrast to the standard PSI approach[8,10], this PSI method does not require any a priori assumptions about the temporal nature of the deformation for PS selection. This is achieved by using the spatially correlated nature of deformation rather than requiring a known temporal dependence. More details about the way that StaMPS identifies PS from interferograms can be found in[16,17,18]. The SB method uses amplitude dispersion values and then identifies the SDFP pixels performing phase analysis in space and time. Because PSI and SB approaches are optimized for resolution elements with different

scattering characteristics, they are complementary, and techniques that combine both approaches are able to extract the signal with greater coverage than either method alone[15,19]. Thus, both selections (PS + SDPF) are combined and a 3D phase unwrapping algorithm is applied to isolate the deformation signal, based on these pixels. The inner workings of this software package are described in more detail in[9,15,16,17,18,20,21].

3.2. SARPROZ

This interferometric tool package developed in MATLAB® as well provides many different options for combining long series of data, being able to select different set of interferograms to process and different techniques. Parameters can be estimated through the classical PSI algorithm as well as through the Quasi-PS one. In the end, APS can be estimated through different algorithms for the graph inversion. All details about this interferometric package can be found in[22,23] and on the official website (www.sarproz.com).

As the first step, all the SLCs from the input datasets were converted into the format readable by SARPROZ. Several tasks, such as computation of the dataset statistics (Fig. 2), applying precise orbits (if available), obtaining a weather data for each scene, selecting the subset of SLCs to cover the area of interest, etc. are performed in this step in a simple GUI (Graphic User Interface). The master acquisition for both sensors have been chosen with respect to the StaMPS processing that was performed first. Since SARPROZ automatically downloads the meteorological data for each acquisition date, the precipitation was detected during the day of previously selected master, however, it has not been changed, in order to keep results comparable. Moreover, 2 ERS-1/2 images without precise orbits were omitted due to the bias that they were causing in final estimated parameters, though they were co-registered based on the parameter changes performed within a software GUI. Master image and slave images were then extracted and co-registered. Within the co-registration process, the offsets between the master and slave images are estimated by investigating the correlation of the amplitude information in the spatial and spectral domain. Each slave image is aligned to the master, so that the portion of imaged terrain of each pixel in the slave image is the same in the corresponding pixels of the master image. From the co-registered stack of images, the reflectivity map, as the temporal average of the intensities of all images in a dataset was generated and the amplitude stability index was computed[24]. The initial coarse set of points for further processing is selected, possibly detecting and ignoring sidelobe observations[25]. The preliminary geocoding using 25 m DEM[26] was performed next. Importantly to note, very precise geolocation of each PS (Persistent Scatterer) point could be obtained due to proprietary procedures implemented in SARPROZ[27,28]. The geocoding could be done either automatically or manually. Depending on the available data and the resolution, there are different strategies for selecting good tie-points for geocoding. Lamp posts clearly identifiable in reflectivity maps from both tracks have been chosen manually as ground control point (GCP) in our case. Next, the DEM in SAR coordinates was calculated to assist the PSI processing. Finally, the phase to height and phase to flat constants were generated.

From then on, the processing was carried out on a set of points exploiting a different characteristic related to the amplitude of the radar signal (reflectivity map, amplitude stability index), temporal and spatial coherence[29]. For creating a network of PS candidates (PSC) a threshold on amplitude stability index was applied in order to estimate preliminary parameters and Atmospheric Phase Screen (APS). The larger set of points based on reflectivity map and spatial coherence[29] was used during the compensation of APS. Inverted residuals APS[30] were estimated using the stratification option in order to estimate the correlation between APS and elevation DEM, compensating the vertical stratification of the APS for the coherent points in different altitudes over mostly mountainous area. After APS removal the final estimates of height and velocity were computed. As a result, 32 and 26 images have been used for the analysis of ERS-1/2 and Envisat datasets respectively in SARPROZ, in comparison to 24 and 27 images selected in StaMPS as during the re-evaluation of the unwrapping errors in interferometric pairs with higher perpendicular baselines the SLC images were excluded in StaMPS subsequently. The threshold on temporal coherence and spatial coherence value was used to visualize the final results. Reference point for both processing stacks was chosen with respect to previous StaMPS processing in stable places indicated by geologists (Sierra Gorda, Fig. 1). These areas are exhibiting maximum values of temporal and spatial coherence in results from SARPROZ, underlining the assumption that they are not undergoing any major movements.

3.3. The P-SBAS Web Tool within the G-POD Environment

G-POD is an environment that was designed by ESA within the Research & Service Support[31] with applications that exploit Earth Observation (EO) data. In such environment, a generic application can be encapsulated within such a virtual environment and can exploit both distributed high-performance processing resources and large volumes of archived data, in order to provide the scientific community with new EO services[32].

G-POD benefits from the access to the ESA computing facilities as well as to their EO data archives, and provides a friendly web user interface that permits the processing of jobs on a distributed computing system. The G-POD environment is, indeed, a complex distributed architecture that is constituted of different logical subsystems, such as computing facility, web portal, services modules repository, and satellite data catalogues.

The P-SBAS web tool within G-POD is a totally automatic approach that allows processing the full P-SBAS workflow (Fig.3), and it only requires the selection, from the ESA archives, of SAR data to be exploited, and the setting of few parameters needed for the MT-InSAR processing. This G-POD service integrates the multi-temporal and DInSAR algorithm developed by CNR-IREA, adapted for parallel computation[33].

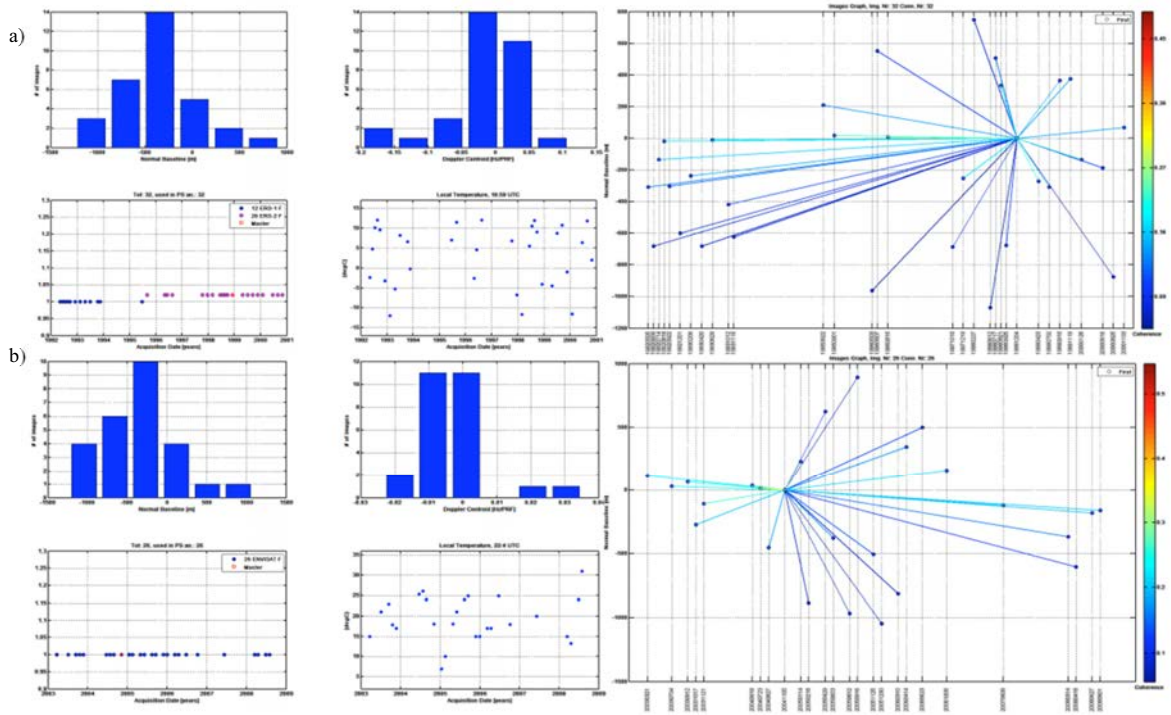

Fig. 2. On the left sided part of the figures a) ERS-1/2 descending track 51, and b) Envisat ascending track 459, in clockwise order, depicted are the histogram of the perpendicular baselines, the histogram of the Doppler centroids, the temperature at the acquisition time and the time sampling of the acquisitions and sensors that acquired the data. On the right sided part, the interferometric configuration for the PSInSAR analysis.

The P-SBAS Service allows any user to produce multi-temporal DInSAR products. More specifically, the user must carry out the following actions in order to create a valid G-POD task:

- Select the area of interest (AOI) to be processed and the DInSAR reference pixel. The AOI selection is made via a bounding box over an interactive geographical map client. Instead, the reference point selection is carried out by shifting a place mark over the map client. It is also possible to insert geographic coordinates of a known point in the appropriate fields. As a general hint for the reference point selection, it is strongly suggested that it is located in a stable and (expected) coherent area;
- Indicate the time period used for the subsequent SAR data querying;

- Select the ESA data catalogue from which the SAR acquisitions are automatically retrieved. The Virtual Archive 4 (VA4) catalogue[34] is the main source of SAR data for the P-SBAS web tool. VA4 is composed by subsections containing the ENVISAT ASAR and the ERS-1/2 data, the latter being present in both CEOS and ASAR formats. Moreover the possibility to select data by relative orbit number (track) is also provided;
- Save task in workspace to create the tasks without start the processing, or press the Process it button to immediately start the processing

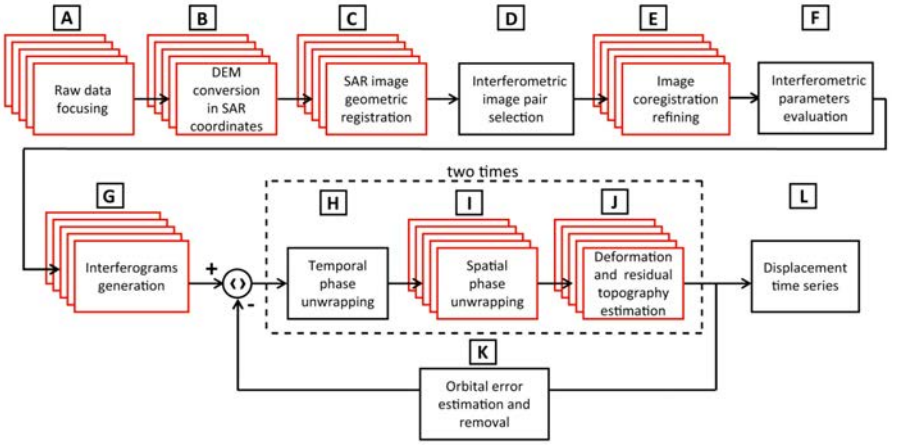

Fig. 3. P-SBAS workflow. Black/single and red/multilayered blocks represent sequential and parallel (from a process-level perspective) processing steps, respectively. This scheme reduces to the SBAS sequential workflow when only one processor is employed. From[33].

Optionally, some basic interferometric SAR parameters to define are: spatial and temporal baseline thresholds, approximate size (in meters) of the resulting ground pixel, filtering coefficient and noise thresholds. It is strongly suggested that expert users on DInSAR processing perform the setting of these parameters. However, to simplify this task for less expert users, default values for each parameter are also provided. It is worth highlighting that these default values are the result of extensive and long-term analyses of ESA C-band data and are suitable for a large part of case studies. Note that a flag is also available to limit the DInSAR analysis to the generation of multi-temporal interferograms only.

Once the aforementioned actions have been done, the user can run the P-SBAS processing chain on the allocated computing facilities. While running, the user can also monitor the processing status and, once the job is terminated, the final results are available for download from: (i) either the G-POD web portal or; (ii) a user-defined FTP server.

4. Results and conclusions

Figs. 4 and 5 show the mean LOS velocity maps derived from StaMPS, SARPROZ and P-SBAS processing for ERS-1/2 and Envisat ASAR dataset respectively. In the case of P-SBAS results, very few PS are detected in Sierra Tejeda. This makes comparisons with the other tool results somewhat difficult in order to identify similar deformation patterns.

Reviewing the deformation maps, several places with suspicious deformation trends have been identified. As it is sometimes complicated to resolve imperfections in supposed model for estimated parameters over wide areas (e.g. atmospheric disturbances, un-modeled deformation, etc.), these sites would require deeper investigation in terms of processing them locally, where some of these imperfections can be minimized or even neglected (atmospheric effects to the extent of 5x5 km^2 [10]). For the case of SARPROZ, different tests, involving redundant PSC (Permanent Scatterer Candidates) networks and redundant images' graph connections[30] in order to increase robustness and study various decorrelation mechanisms are under examination. It is worth to mention, from most of the InSAR tool packages available to scientific community, that SARPROZ allows for seamless transition between many different interferometric strategies (images graph connections, weights on a coherence, different parameters for a-priori and a-posteriori selection of the points, incorporating the life-time of the targets, etc.) in search for the signal of interest

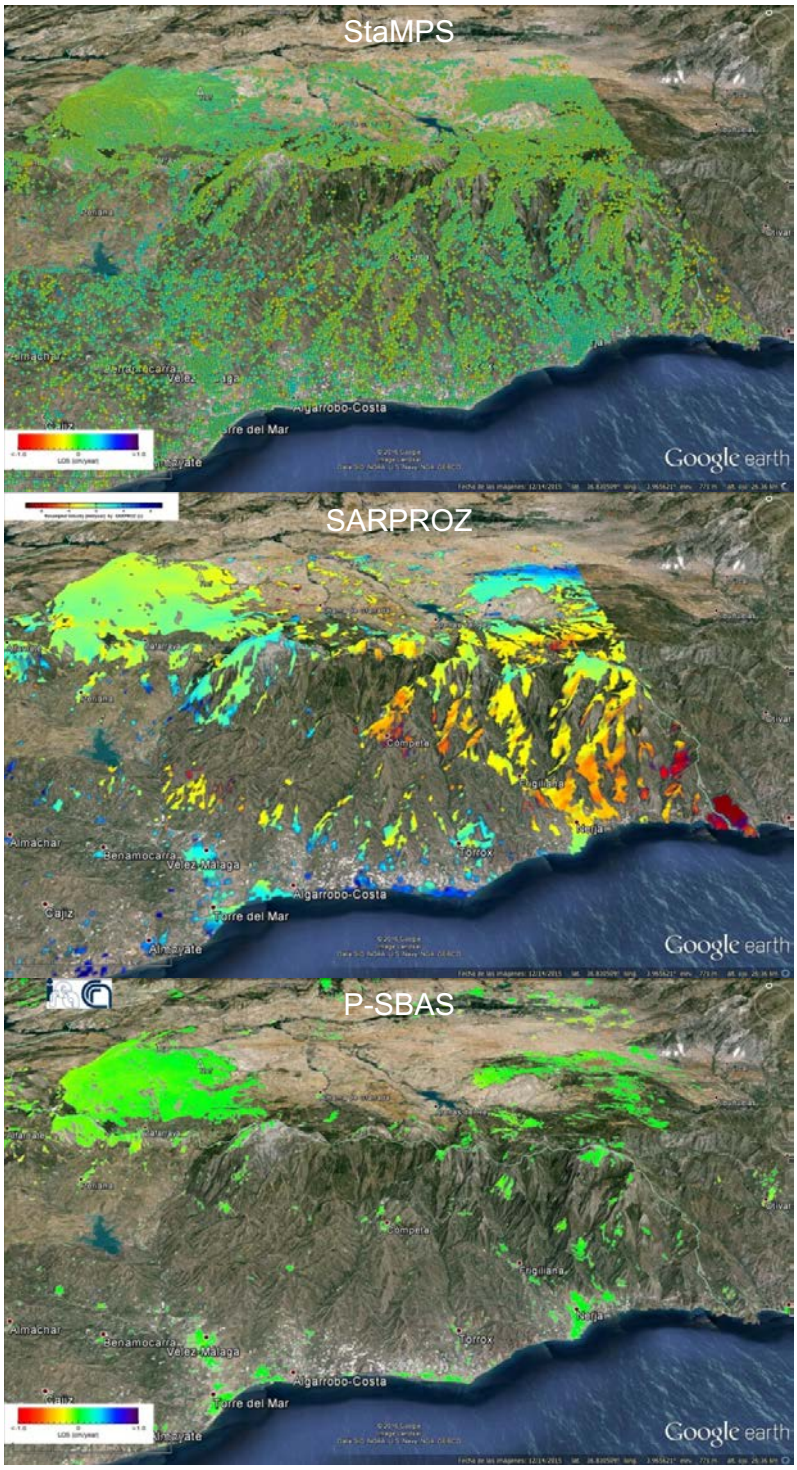

Fig. 4. 3D view of the mean LOS velocity maps for ERS-1/2 (1992-2000) from StaMPS (top), SARPROZ (middle), and P-SBAS (bottom). Velocity range is in the interval of -10 to 10 mm/yr.

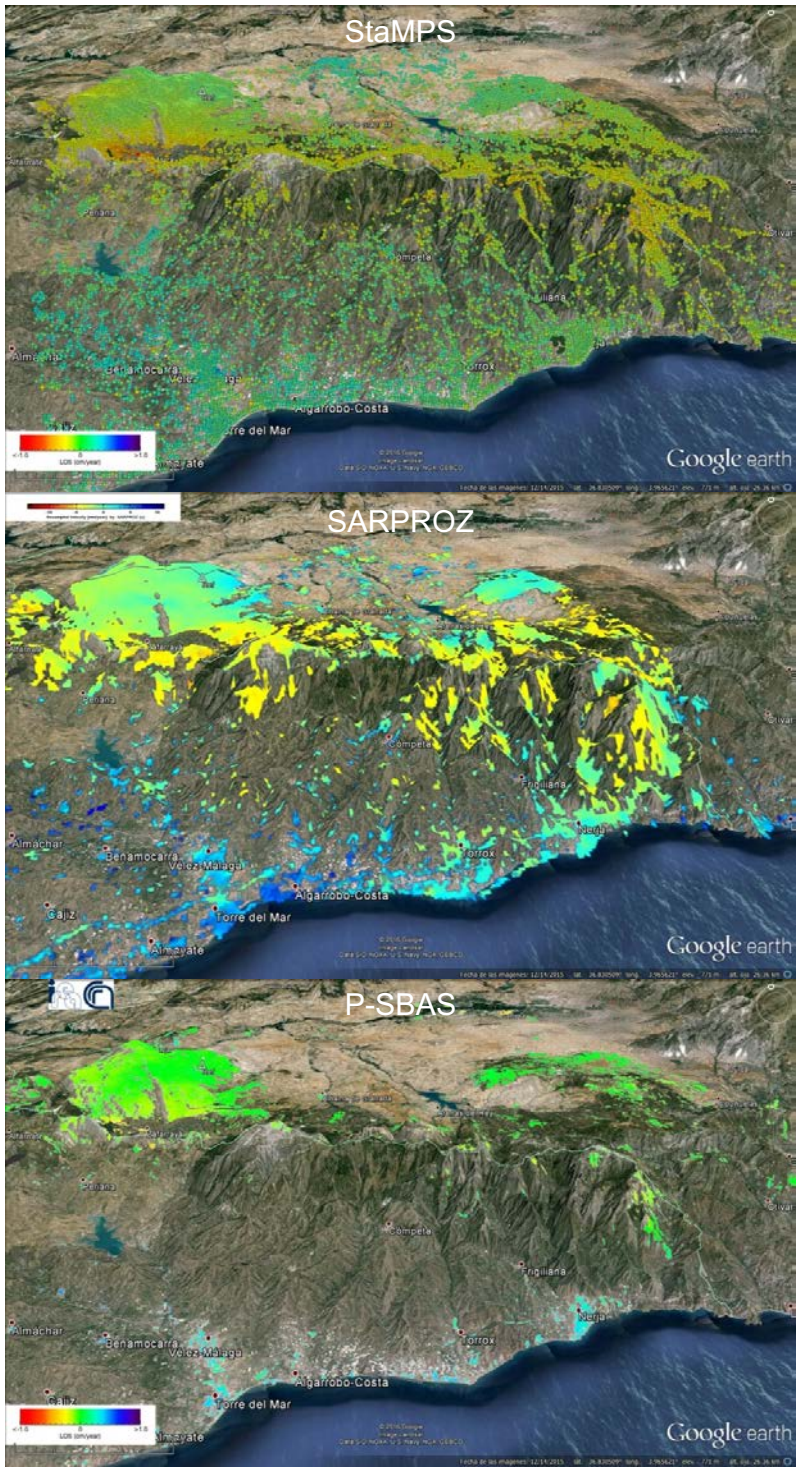

Fig. 5. 3D view of the mean LOS velocity maps for Envisat ASAR (2003-2008) from StaMPS (top), SARPROZ (middle), and P-SBAS (bottom). Velocity range is in the interval of -10 to 10 mm/yr.

whereas the default options and user-friendly interface allow beginners to easily tackle the interferometry.

In general, the deformation patterns from StaMPS and SARPROZ are very similar in both periods (from 1992 to 2008). The SARPROZ results thus confirm these obtained by[5] using StaMPS and, as a consequence, and that the main elevation areas undergone present-day subsidence for all the period of analysis.

Acknowledgements

SAR data are provided by the European Space Agency (ESA) in the scope of 28654 G-POD and 7629 CAT-1 project. This research was supported by ESP2006-28463-E and PRX14/00340 projects from Ministerio de Ciencia e Innovación (Spain). In addition, it was supported by the UJA2015/08/05 and CEACTierra projects from University of Jaén (Spain) and the RNM-282 research group from the Junta de Andalucía (Spain). Data have been processed by DORIS from TUDelft, StaMPS, SARPROZ (Copyright (c) 2009-2016 Daniele Perissin) and G-POD service of ESA. The authors want to thank the support provided by the Research and Service Support team of the European Space Agency (ESA) for the processing resources and data access provided for the pre-processing of the satellite images through the Grid Processing on Demand service. The results were visualised in MATLAB® using Google Maps™ and Google Earth™. The work has been supported also by the Slovak Grant Agency VEGA under projects No. 1/0714/15 and 1/0462/16.

References

1. Usai S. The use of man-made features for long time scale INSAR. Geoscience and Remote Sensing, 1997. IGARSS '97. Remote Sensing - A Scientific Vision for Sustainable Development, 1997 IEEE International, 4, p. 1542-1544.
2. Usai S, Hanssen R. Long time scale INSAR by means of high coherence features. 3rd ERS Symposium on Space at the service of our Environment, Florence, Italy, 14-21 March, European Space Agency. 1997.
3. Crosetto M, Montserrat O, Cuevas-González, M, Devanthéry N, Crippa B. Persistent Scatterer Interferometry: A review. *ISPRS J Photogramm* 2015, http://dx.doi.org/10.1016/j.isprsjprs.2015.10.011
4. De Mets C, Gordon RG, Argus DF, Stein S. Current plate motions. *Geophys J Int*, 1990; 101:425– 478.
5. Ruiz-Armenteros AM, Delgado JM, Sousa JJ, Hanssen RF, Caro M, Gil AJ, Galindo-Zaldívar J, Sanz de Galdeano C. Deformation monitoring in Zafarraya fault and Sierra Tejeda Antiform (Betic Cordillera, Spain) using satellite radar interferometry. In: FRINGE 2015 – Advances in the Science and Applications of SAR Interferometry and Sentinel-1 InSAR Workshop, 23-27 marzo 2015, ESA-ESRIN (Frascati, Italia). Noordwijk: ESA Communications SP-731 CD-ROM; 2015.
6. http://www.irea.cnr.it (accessed on 3 June 2016).
7. http://wiki.services.eoportal.org/rss-portal.php (accessed on 3 June 2016).
8. Ferretti A, Prati C, Rocca F. Permanent Scatters in SAR Interferometry. *IEEE Geosci Remote* 2001;39,1:8-20.
9. Hooper A, Zebker H, Segall P, Kampes B. A new method for measuring deformation on volcanoes and other natural terrains using InSAR persistent scatterers. *Geophys Res Lett* 2004;31: L23611. doi:10.1029/2004GL021737.
10. Kampes BM. *Radar Interferometry: Persistent Scatterer Technique*, Kluwer Academic Publishers, Dordrecht, The Netherlands; 2006.
11. Berardino P, Fornaro G, Lanari R, Sansosti E. A new algorithm for surface deformation monitoring based on small baseline differ-ential SAR interferograms. *IEEE Geosci Remote* 2002;40(11), 2375 – 83.
12. Schmidt DA, Bürgmann R. Time-dependent land uplift and subsidence in the Santa Clara valley, California, from a large interferometric synthetic aperture radar data set. J. Geophys. Res. 2003:108,B9:2416–2428.
13. Hooper A, Bekaert DPS, Spaans K, Arikan M. Recent advances in SAR interferometry time series analysis for measuring crustal deformation. *Tectonophysics* 2002;514-517:1-13. doi:10.1016/j.tecto.2011.10.013.
14. Hooper A, Bekaerti D, Spaans K. *StaMPS/MTI Manual*. Version 3.3b1. School of Earth and Environment. University of Leeds, United Kingdom; 2013.
15. Hooper A. A multi-temporal InSAR method incorporating both persistent scatterer and small baseline approaches. *Geophys Res Lett* 2008;35:L16302. doi:10.1029/2008GL034654.
16. Hooper A, Segall P, Zebker H. Persistent Scatterer InSAR for Crustal Deformation Analysis, with Application to Volcán Alcedo, Galapagos, *J Gephys Res*, 2007;112, B07407, doi:10.1029/2006JB004763.
17. Sousa J, Ruiz A, Hanssen R, Bastos L, Gil A, Galindo-Zaldívar J, Sanz de Galdeano C. PS-InSAR processing methodologies in the detection of field surface deformation - study of the Granada Basin (Central Betic Cordilleras, Southern Spain). *J Geodyn* 2010;49: 181-189 doi:10.1016/j.jog.2009.12.002.
18. Sousa J, Hooper A, Hanssen R, Bastos L, Ruiz A. Persistent Scatterer InSAR: A comparison of methodologies based on a model of temporal deformation vs. spatial correlation selection criteria. *Remote Sens Environ* 2011;115(10):2652-2663.
19. Ferretti A, Fumagalli A, Novali F, Prati C, Rocca F, Rucci A. A new algorithm for processing interferometric data-stacks: SqueeSAR. *IEEE Geosci Remote* 2011;49:3460-3470.
20. Hooper A. A statistical-cost approach to unwrapping the phase of InSAR time series. European Space Agency (Special Publication) ESA SP-

677. 2010.
21. Hooper AJ. *Persistent scatterer radar interferometry for crustal deformation studies and modelling of volcanic deformation.* Ph.D. thesis, Stanford University; 2006.
22. Perissin D, Wang T. Repeat-Pass SAR Interferometry with Partially Coherent Targets. *IEEE Geosci Remote* 2012;50,271-280.
23. Perissin D, Wang Z, Wang T. *The SARPROZ InSAR tool for urban subsidence/manmade structure stability monitoring in China*. Proc. of ISRSE 2010, Sidney, Australia, 10-15 April 2011.
24. Lei L, Perissin D, Qin Y. Change Detection with Spaceborne InSAR Techniques in Hong Kong. In: *Proc. of IGARSS 2013*, Melbourne (Australia), 2013.
25. Perissin, D. *SAR super-resolution and characterization of urban targets*. Ph.D. thesis. Italy: Politecnico di Milano; 2006.
26. http://www.ign.es/ign/layoutIn/modeloDigitalTerreno.do (accessed on 3 June 2016).
27. Perissin D, Rocca F. High Accuracy Urban DEM Using Permanent Scatterers. *IEEE Geosci Remote* 2006;**44**,3338 – 3347.
28. Perissin D, Ferretti A. Urban target recognition by means of repeated spaceborne SAR images, *IEEE Geosci Remote* 2007, **45**,12,December 2007:4043 - 4058.
29. Perissin D, Wang T (2012). Repeat-Pass SAR Interferometry with Partially Coherent Targets. *IEEE Geosci Remote* 2012;**50**,1:271–280.
30. Perissin D. *SARPROZ software manual*. Official Product Web Page: http://www.sarproz.com; 2016.
31. Marchetti PG, Rivolta G, D'elia S, Farres J, Gobron N, Mason G. A Model for the Scientific Exploitation of Earth Observation Missions: The ESA Research and Service Support. *IEEE Geosci Newsl* 2012;**162**,10–18.
32. GRID Processing on Demand. Available online: http://gpod.eo.esa.int (accessed on 6 June 2016).
33. Casu F, Elefante S, Imperatore P, Zinno I, Manunta M, De Luca C, Lanari R. SBAS-DInSAR Parallel Processing for Deformation Time-Series Computation. *IEEE J Sel Top Appl* 2014; **7**, 8:3285-3296, Aug. 2014. doi: 10.1109/JSTARS.2014.2322671.
34. Virtual Archive 4. Available online: http://eo-virtual-archive4.esa.int (accessed on 3 June 2016).